The measurement of ultrasound scattering from individual micron-sized objects and its application in single cell scattering

Omar Falou[a)]
Department of Electrical and Computer Engineering, Ryerson University, 350 Victoria Street, Toronto, Ontario M5B 2K3, Canada

Min Rui
Department of Physics, Ryerson University, 350 Victoria Street, Toronto, Ontario M5B 2K3, Canada

Ahmed El Kaffas
Department of Medical Biophysics, University of Toronto, 610 University Avenue, Toronto, Ontario M5G 2M9, Canada

J. Carl Kumaradas and Michael C. Kolios
Department of Physics, Ryerson University, 350 Victoria Street, Toronto, Ontario M5B 2K3, Canada

(Received 14 January 2010; revised 17 May 2010; accepted 18 May 2010)

The measurement of the ultrasound backscatter from individual micron-sized objects such as cells is required for various applications such as tissue characterization. However, performing such a measurement remains a challenge. For example, the presence of air bubbles in a suspension of cells during the measurements may lead to the incorrect interpretation of the acoustic signals. This work introduces a technique for measuring the ultrasound backscatter from individual micron-sized objects by combining a microinjection system with a co-registered optical microscope and an ultrasound imaging device. This allowed the measurement of the ultrasound backscatter response from a single object under optical microscope guidance. The optical and ultrasonic data were used to determine the size of the object and to deduce its backscatter responses, respectively. In order to calibrate the system, the backscatter frequency responses from polystyrene microspheres were measured and compared to theoretical predictions. A very good agreement was found between the measured backscatter responses of individual microspheres and theoretical predictions of an elastic sphere. The backscatter responses from single OCI-AML-5 cells were also investigated. It was found that the backscatter responses from AML cells are best modeled using the fluid sphere model. The advantages, limitations, and future applications of the developed technique are discussed.
 [DOI: 10.1121/1.3455795]

PACS number(s): 43.80.Cs, 43.80.Ev, 43.20.Fn, 43.40.Fz [CCC] Pages: 894–902

I. INTRODUCTION

The measurement of the ultrasound backscatter from individual micron-sized objects such as cells is needed for applications ranging from tissue characterization to molecular imaging. This has been previously done by scanning a sample with objects in suspension and analyzing the brightest signals received, assuming these to be caused by scattering events from the single objects of interest (Baddour *et al.*, 2005; Baddour and Kolios, 2007; Falou *et al.*, 2008). This technique is error-prone since the bright signals may be from unwanted particles in the suspension, aggregates of the objects of interest (e.g., a cluster of cells), or from air bubbles, which are hard to eliminate from fluid suspensions. This work introduces a new technique, consisting of a microinjection system and co-registered optical and ultrasonic imaging devices, to measure the ultrasound backscatter from single micron-sized objects.

It has been shown that high frequency ultrasound (20–60 MHz) can be used to detect structural and physical changes in cell ensembles during cell death through apoptosis (Czarnota *et al.*, 1997; Czarnota *et al.*, 1999; Kolios *et al.*, 2004). Ultrasonic backscatter from cell ensembles treated with the chemotherapeutic drug cisplatin (which induces apoptosis) increase the ultrasound backscatter signal amplitude by 9–13 dB and lead to changes in the frequency dependence of backscatter. Recent studies showed similar effects after cancer radiotherapy *in vitro* (Vlad *et al.*, 2008) and *in vivo* (Vlad *et al.*, 2009).

Apoptosis, or programmed cell death, was originally defined by Kerr *et al.* (1972) and is characterized by large changes in the structure of the cell: nuclear condensation and DNA degradation, cytoplasm shrinkage, and fragmentation of the cell into membrane-bound bodies (Häcker, 2000; Saraste and Pulkki, 2000). When compared to clinical ultrasound imaging (1–10 MHz), high frequency ultrasound imaging, whose wavelength approaches the size of the cell, is more sensitive to cell structural and spatial distribution changes (Hunt *et al.*, 2002; Tunis *et al.*, 2005). The long term goal of this work is to use high frequency ultrasound imag-

a)Author to whom correspondence should be addressed. Electronic mail: ofalou@ryerson.ca

ing to determine the apoptotic index, the percentage of cells in a volume undergoing apoptosis, which will help in quantifying patient response to cancer treatment. However, a theoretical model of ultrasound scattering from cell ensembles is required in order to determine the proportion of cells undergoing apoptosis in a tumor and hence assess the effectiveness of therapy.

Most scattering models used for lower frequency ultrasonic tissue characterization assume a random distribution of scatterers and a Gaussian-like variation in tissue acoustic properties (Lizzi *et al.*, 1983; Insana and Hall, 1990; Oelze *et al.*, 2002). These models have been used to diagnose various tissue pathologic states (Lizzi *et al.*, 1988; Lizzi *et al.*, 1997; Ursea *et al.*, 1998; Feleppa *et al.*, 2000; Mamou *et al.*, 2006). However, most tumor tissues exhibit non-random spatial cell distributions, and hence the need for more accurate scattering models. A prerequisite to these models is the understanding of the backscatter responses at the cellular level.

Recently, Baddour *et al.* (2005) and Baddour and Kolios (2007) performed measurements of high frequency ultrasound backscatter responses from single eukaryotic cells in suspension. They found that for prostate carcinoma (PC-3) cells whose nucleus to cell volume ratio is 0.33, the ultrasound backscatter could be modeled as a fluid sphere (Baddour and Kolios, 2007). Falou *et al.* (2008) presented similar findings for non-nucleated biological specimens, such as sea urchin oocytes. However, for human acute myeloid leukemia (OCI-AML-5) cells whose nucleus to cell volume ratio is 0.5, Baddour and Kolios (2007) found that the ultrasound backscatter response could not accurately be modeled as a fluid sphere. They hypothesized that for cells with low nucleus to cell volume ratios (e.g., PC-3), the backscatter response can be modeled as a fluid sphere. However, for cells with a nucleus to cell volume ratio of 0.5 (e.g., OCI-AML-5), the backscatter response is better modeled as an elastic sphere. During their experiments, no visual confirmation of the underlying scattering structures could be made, as the ultrasound measurements were done with cells in suspension. In addition, the possible presence of air bubbles in the suspension of cells may have led to the incorrect interpretation of the measured ultrasonic signals.

In this work, a new technique is developed to measure the exact ultrasonic backscatter response from individual micron-sized objects, particularly OCI-AML-5 cells. This method allows the optical detection of the scattering objects responsible for the backscatter responses measured by the ultrasound imaging devices as optical videos of the scattering objects are made during the ultrasound acquisition. Using this new setup, the ultrasonic behavior of acute myeloid leukemia cells was investigated by comparing the measured backscatter response to theoretical predictions from a fluid sphere model (Anderson, 1950). It was found that for these cells, the backscatter response at 12–57 MHz was best modeled as a fluid sphere.

II. TECHNIQUE DESCRIPTION AND VALIDATION

A. Methods

A XenoWorks microinjection system (Sutter Instrument Co., Novato, CA) consisting of a digital microinjector, a micromanipulator, and a P-97 micropipette puller was used. The system uses custom tailored micropipettes with pressure values ranging from −35 kPa to +35 kPa, controllable in 0.7 kPa increments, applied along the surface of the object of interest. Fire-polished thin wall borosilicate micropipettes of length, outer diameter, and inner diameter of 10, 1, and 0.78 mm, respectively (Sutter Instrument Co., catalog number: BF100-78-10) were pulled to form tips of outer and inner diameters of 5 and 3 μm, respectively. The micropipette movement was controlled by a joystick with a translational precision of 50/100 μm at the micropipette tip for every full rotation/swing of the joystick, along each of the x, y, and z axes. A Retiga EXi CCD camera (QImaging, Inc., Surrey, BC) mounted on an Olympus IX71 inverted microscope (Olympus America, Inc., Center Valley, PA) and a VEVO770 ultrasound imaging device (VisualSonics, Inc., Toronto, ON) were used to capture optical and ultrasonic data, respectively. Both devices were connected to a PC loaded with STREAMPIX 3 (NorPix, Inc., Montreal, QC), a digital video recording software and the image analysis tool, IMAGEJ (http://rsbweb.nih.gov/ij/), which allowed for the capturing of optical movies (frame rate of 9 frames per second) and size measurements of the object of interest. The MATLAB 7 software package (The MathWorks, Inc., Natick, MA) was used to process the ultrasonic data.

TABLE I. Properties of the transducers used in the experiments

Transducer	f-number	Focal length (mm)	−6 dB bandwidth (MHz)
25 MHz polyvinylidene fluoride (RMV-710B)	2.1	15	12–28
55 MHz polyvinylidene fluoride (RMV-708)	2.25	4.5	25–57

Ultrasonic data acquisition was performed using a VEVO770 ultrasound imaging device. Radiofrequency data were collected at a sampling rate of 420 MHz. Two broadband focused Polyvinylidene Fluoride transducers (RMV-710B and RMV-708), with different resonant frequencies, f-numbers, and focal lengths, were employed. Table I summarizes the properties of the two transducers. Only data from the −6 dB bandwidth of each transducer were used in the analysis which gave an overall bandwidth spanning 12–57 MHz.

A sparse suspension of the scatterer was prepared at room temperature by mixing a very low concentration of scatterers (between 1000 and 10,000 scatterers/ml) into 250 ml of the suspending fluid. The suspension was placed in a custom made container made of plexiglass. The container has a two inch optical window in the bottom and a sleeve which holds the ultrasound transducer at 45 degrees from the vertical as shown in Fig. 1. The transducer axis pointed just above the center of the window and the transducer could be translated along its axis to adjust for a variable focal length. The center of the window was positioned at the focal point of the optical microscope and an individual scattering object was held with the micropipette at the same position. In this manner, optical and ultrasound images were obtained at the

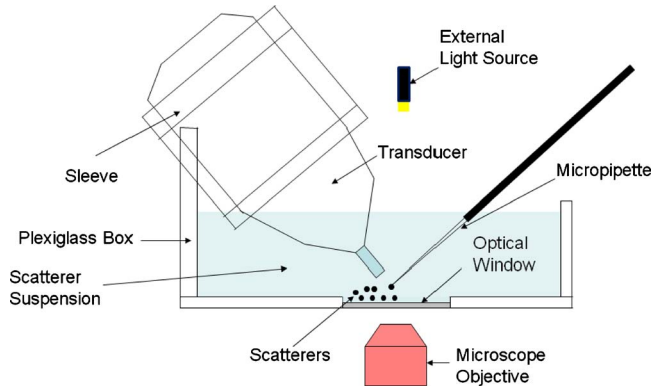

FIG. 1. (Color online) Schematic diagram of the experimental setup. A suspension of the scatterer was placed in a custom made container. The micropipette and the transducer are held perpendicular to one another.

same time. The long axis of the micropipette and the transducer axis were oriented perpendicular to one another. This orientation was important in order to minimize the ultrasonic signal from the micropipette. Initially, the micropipette was brought to the focus of the transducer and its location was saved. It was then translated to the bottom of the container and brought in close proximity of the scatterer. The scatterer was then attached to the micropipette under optical guidance using a pressure ranging from −18.9 kPa to −9 kPa. The micropipette was transferred back to its saved location and the scatterer was released (by using positive pressure of +35 kPa and/or tapping gently on the micropipette) while simultaneously imaging it optically and ultrasonically. Ultrasonic data acquisition was initiated prior to the release of the scatterer from the micropipette.

30 ultrasonic raw RF lines spaced 55–70 μm apart were acquired from different lateral positions for each ultrasound frame and their corresponding B-scans, represented by the matrix $H_{\text{expr\_f}}(t)$, were constructed using the following equation:

$$H_{\text{expr\_f}}(t) = \ln(|\mathsf{H}\{r_{\text{expr\_f}}(t)\}|), \tag{1}$$

where $\mathsf{H}\{\ \}$ is the Hilbert transform and $r_{\text{expr\_f}}(t)$ is the matrix containing measured RF lines for a series of frames. Visual inspection was performed to determine the frames that contained a scatterer. Once a frame containing a scatterer was found, the RF line containing the maximum amplitude was chosen and a hamming window centered at that amplitude was applied in order to minimize the scattering from the micropipette. Figure 2 illustrates the steps taken to deduce the RF line containing the pulse from a single scatterer (in this example, OCI-AML-5 cell suspended in degassed PBS). It shows representative optical images, B-scans, and ultrasonic echoes at 55 MHz of a micropipette before and after the release of scatterer. Optical images and B-scans of the region of interest, containing the micropipette and the scatterer before and after the release of the scatterer are given in Figs. 2(a)–2(d), respectively. Figures 2(e) and 2(f) illustrate

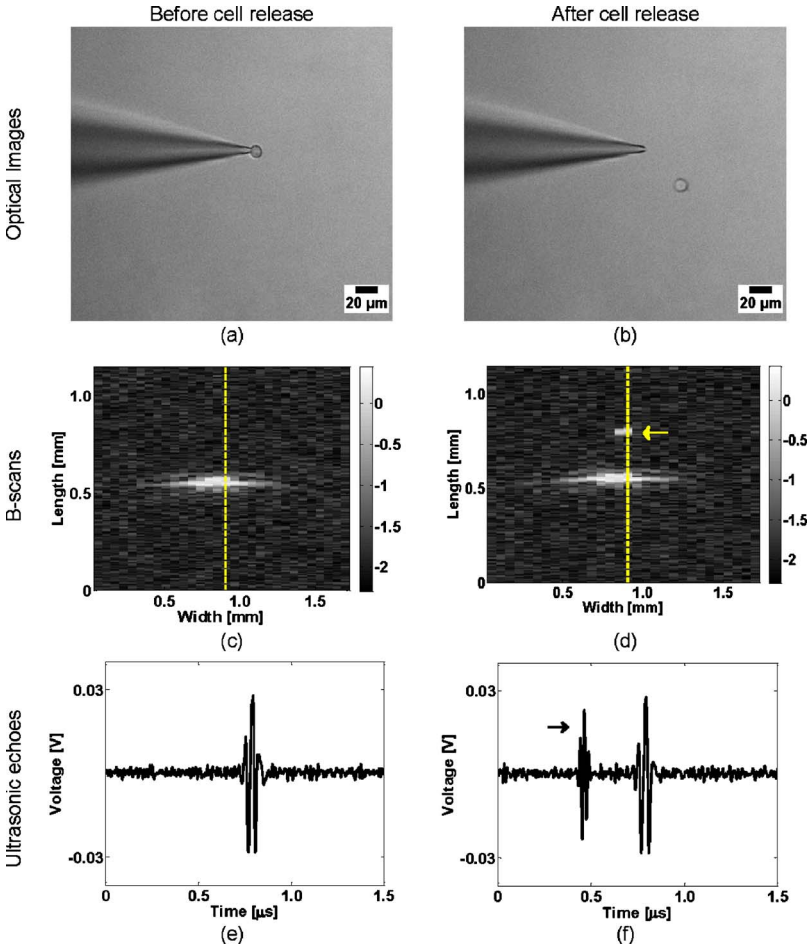

FIG. 2. (Color online) Representative optical images, B-scans, and ultrasonic echoes at 55 MHz of a micropipette before [(a),(c),(e)] and after the release of a scatterer (OCI-AML-5 cell) [(b),(d),(f)]. (c) and (d) are the B-scans of the region of interest, containing the micropipette and the released scatterer. (e) and (f) represent the backscattered pulses at the dashed lines in figures (c) and (d), respectively. The arrow points to the scatterer in (d) and the RF echo from the scatterer in (f).

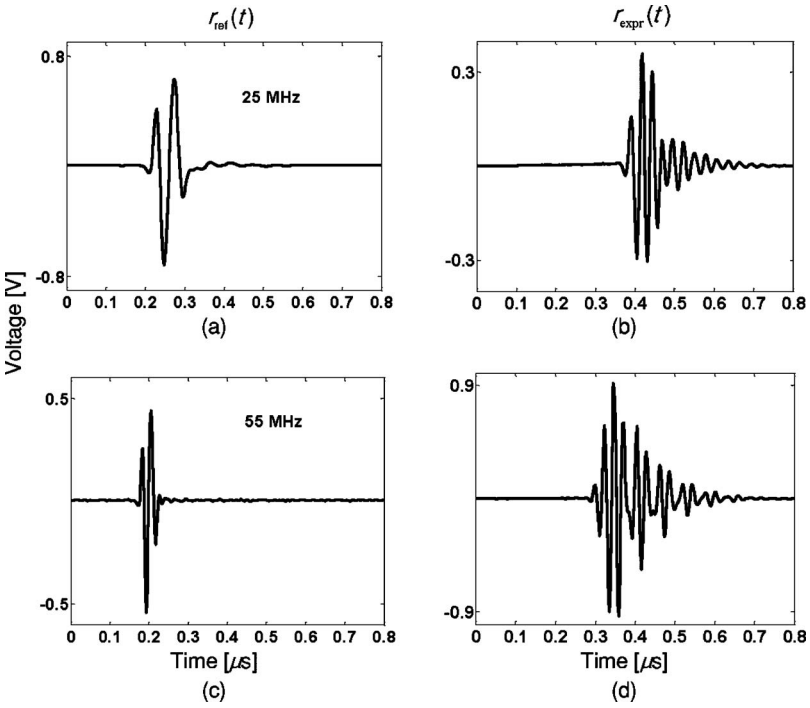

FIG. 3. Representative backscatter echoes from a 20 μm polystyrene microsphere and their corresponding incident pulses (as measured by the reflection from the surface of Dow Corning fluid at the transducer focus): incident pulses at (a) 25 and (c) 55 MHz; echoes from a 20 μm polystyrene microsphere at (b) 25 and (d) 55 MHz.

the backscattered pulses at the dashed lines in Figs. 2(c) and 2(d), respectively.

The backscatter transfer function, $\mathrm{BSTF}_{\mathrm{expr}}(\omega)$, was calculated as:

$$\mathrm{BSTF}_{\mathrm{expr}}(\omega) = \frac{R_{\mathrm{expr}}(\omega)}{R_{\mathrm{coef}} R_{\mathrm{ref}}(\omega)}, \tag{2}$$

where $R_{\mathrm{expr}}(\omega)$ is the Fourier transform of the backscatter signal from a single scatterer. R_{coef} is the reflection coefficient of ultrasound energy incident from the scatterer suspension fluid to a Dow Corning 710 fluid (Applied Industrial Technologies, Cleveland, OH, Part number: 710 4 kg PL; $\rho = 1.11$ g/cm^3, $c = 1370$ m/s) and $R_{\mathrm{ref}}(\omega)$ is the Fourier transform of the "reference signal," which is the measured reflection from the surface of Dow Corning Fluid at the transducer focus, at room temperature. Two different suspension fluids were used in the experiments depending on the scatterer. The $|\mathrm{BSTF}|^2$ are presented in the form of spectral plots expressed in decibels relative to the backscatter intensity from the reference (dB_r). The above procedure was repeated until successful measurements of the BSTF were achieved (success criteria are described in Sec. III).

This method for measuring the backscatter transfer function of micron-sized object was tested with a 20 μm diameter polystyrene microspheres (Beckman Coulter Inc., ref. number: 6602798). These were used because they are homogeneous, spherical and have well-known physical properties. The microspheres were suspended in distilled and degassed water ($\rho = 1.0$ g/ml, $c = 1483$ m/s) at room temperature. Hamming windows of 0.83 and 0.95 μs widths were applied to the 25 and 55 MHz backscatter measurements, respectively, to localize and isolate the signal from the microsphere. The backscatter transfer function, $|\mathrm{BSTF}|^2$, was determined from the measured data and compared to the theoretical backscatter frequency responses calculated for an elastic sphere using the Faran scattering model (Faran, 1951) to validate the new method.

B. Results

Figure 3 shows representative backscatter echoes from a single 20 μm polystyrene microsphere in degassed and distilled water and their corresponding incident pulses at 25 and 55 MHz. The theoretical and averaged experimental backscatter frequency responses within a range that corresponds to the -6 dB bandwidths of each transducer are plotted in Fig. 4. For the theoretical calculations, the elastic sphere were assumed to have the parameters: $\rho = 1.05$ g/ml, $c = 2350$ m/s, $\sigma = 0.35$.

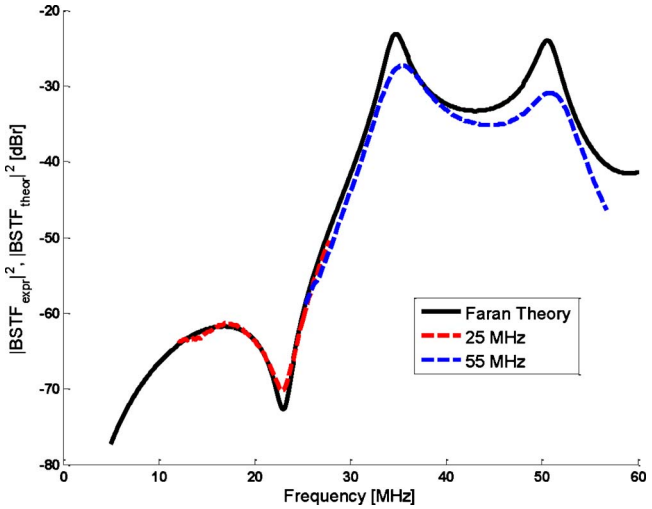

FIG. 4. (Color online) Theoretical and experimental backscatter frequency responses of a single 20 μm polystyrene microsphere in degassed and distilled water subject to incident pulses from two transducers: 25 and 55 MHz (elastic sphere model parameters: $\rho = 1.05$ g/ml, $c = 2350$ m/s, $\sigma = 0.35$).

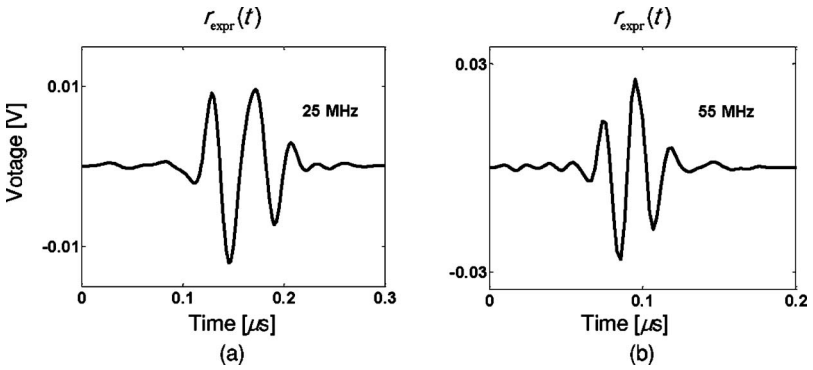

FIG. 5. Representative backscatter echoes from an OCI-AML-5 cell imaged at (a) 25 and (b) 55 MHz.

C. Discussion

The measurement of the ultrasonic response from individual micron-size objects, such as biological cells (weak scatterers) and ultrasound contrast agents (strong scatterers), is required for various applications ranging from ultrasound tissue characterization to molecular imaging. Yet, performing such a measurement remains a challenge. For instance, the possible presence of air bubbles or other foreign objects in a suspension of scatterers during the measurements may lead to the incorrect interpretation of the backscattered signals. Spurious air bubbles were repeatedly seen in the experiments in this work despite our best efforts to degas the solutions in which the experiments were done. In addition, the size and shape of the individual object that produces an ultrasound signal are required as input parameters to theoretical models, yet are hard to be measured experimentally. This novel technique combining a microinjection system and co-registered optical and ultrasonic imaging devices (Fig. 1) made it possible to deduce the exact experimental ultrasound backscatter response from micron-sized objects under optical guidance.

There is a very good agreement in the location of the spectral features for the polystyrene microspheres as shown in Fig. 4. The difference was measured to be less than 1% on average between the experimentally measured backscatter frequency response of individual microspheres and the theoretical frequency response of an elastic sphere. For the 55 MHz data, the experimental curve has lower values for the $|\mathrm{BSTF}|^2$ than that of the theoretical one, particularly at the resonance frequencies. This may be due to the increase of the attenuation at high frequencies. The lower value of the $|\mathrm{BSTF}|^2$ for the second resonant peak in the experimental backscatter response when compared to the first peak is a further indication of the increased effect of attenuation in the backscatter response at high frequencies. An examination of the backscatter echoes from the polystyrene microsphere (Fig. 3) reveals the presence of resonances exhibited in the form of ringing patterns. The ring-down durations for such patterns are of 0.3 and 0.4 μs for the 25 and 55 MHz data, respectively. Such findings are further indications of the resonant behavior of microspheres, which agree well with the Faran's scattering model for elastic spheres (Faran, 1951) and have been measured in the past (Baddour *et al.*, 2005).

III. SCATTERING FROM CELLS

The OCI-AML-5 cells were prepared in a degassed and dilute phosphate buffered saline (PBS) solution (in distilled water: 8 g/l sodium chloride, 0.20 g/l potassium chloride, 0.20 g/l potassium phosphate, 1.15 g/l sodium phosphate, 0.132 g/l calcium chloride, 0.10 g/l magnesium chloride). PBS (assumed to have the same density and speed of sound as those of distilled water) was used since it is non-toxic to cells and it has an osmolarity and ion concentrations critical to cell survival. Hamming windows of 0.33 and 0.24 μs widths were applied to the 25 and 55 MHz backscatter measurements from the cells, respectively, to localize and isolate the signal from the cell. The experimental procedure was repeated until eight successful trials (described later in this section) were collected. Since the mass density of an OCI-AML-5 cell is unknown, the individual measured $|\mathrm{BSTF}|^2$ of a cell in each trial was compared to the theoretical backscatter frequency response calculated for a fluid sphere using the Anderson model (Anderson, 1950), with a diameter as measured optically (Vlad *et al.*, 2008), a sound speed of 1535 m/s (Taggart *et al.*, 2007), and a range of densities from 1.0 to 1.2 g/ml for the cell. The least-squares method was used to determine the mass density that produced the best agreement with their corresponding experimental responses, as detailed in Falou *et al.* (2008). The measured optical diameters and theoretical densities were averaged and used to plot the averaged theoretical fit to experimental data.

Representative backscatter echoes from individual OCI-AML-5 cells imaged at 25 and 55 MHz are shown in Fig. 5. Figures 6 and 7 show the best fitted theoretical (assuming a fluid sphere model) and experimental backscatter frequency responses (within the -6 dB bandwidths of the transducer) of a single OCI-AML-5 cell in PBS subject to incident pulses from a 25 and 55 MHz transducers, respectively. Figure 8 shows the theoretical (fluid sphere model parameters: $d=10.5$ μm, $\rho=1.09$ g/ml, $c=1535$ m/s) and the average experimental backscatter frequency responses of a single OCI-AML-5 cell in PBS subject to incident pulses from two transducers: 25 and 55 MHz. Error bars represent the 95% confidence intervals.

The absence of the ringing patterns in the backscatter echoes from individual OCI-AML-5 cells imaged at 25 and 55 MHz (Fig. 5) is an indication of their fluidlike behavior at high frequencies. The nonexistence of sharp and abrupt peaks in the experimental frequency responses presented in Figs. 6 and 7 further confirms this. This is contrary to the findings reported by Baddour and Kolios (2007) where a sharp dip between 10 and 15 MHz was present in the measured frequency responses from individual OCI-AML-5

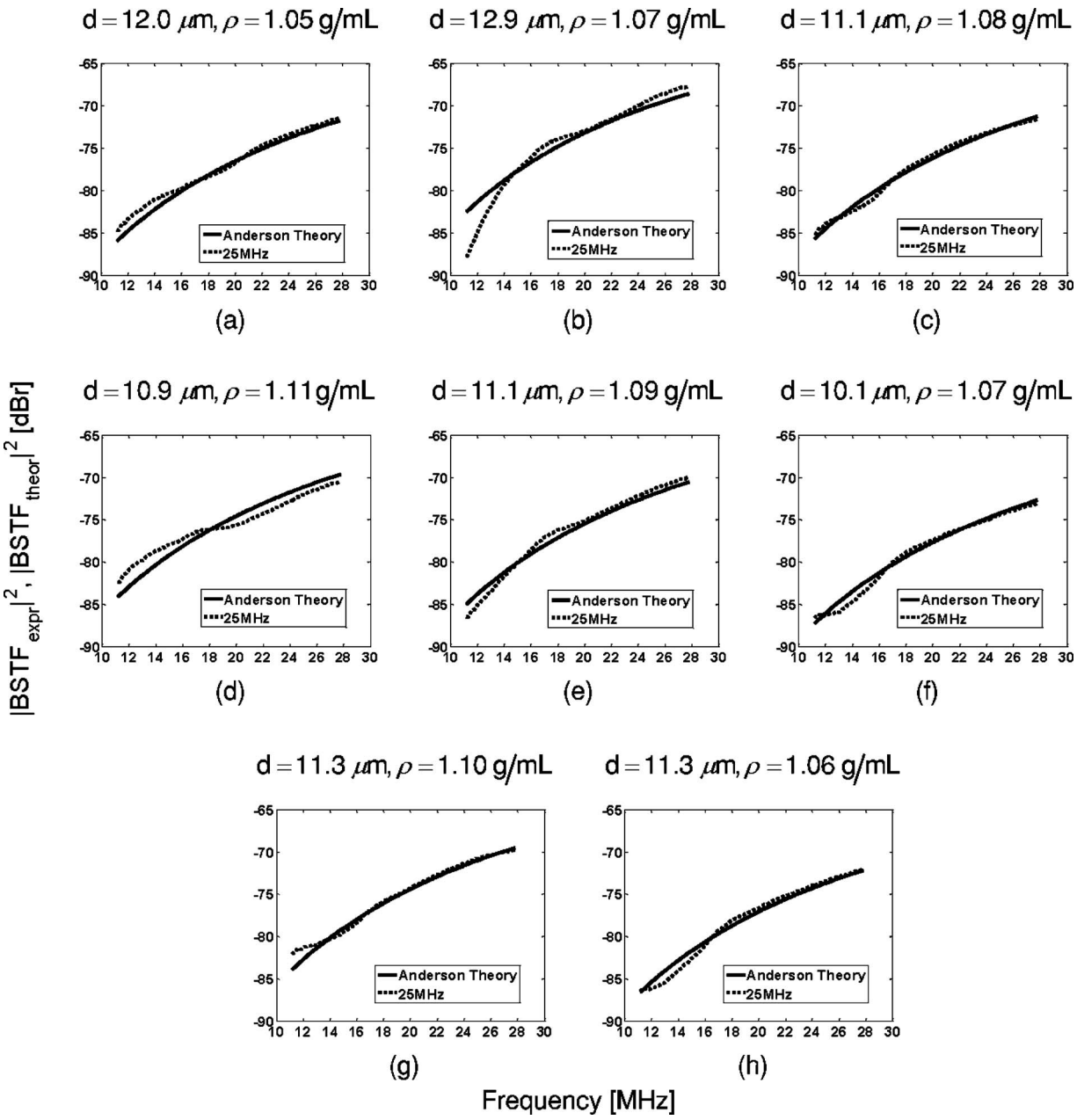

FIG. 6. Theoretical (fluid sphere model: $c=1535$ m/s, diameter and density are given in the figure title) and experimental backscatter frequency responses of a single OCI-AML-5 cell in PBS subject to incident pulses from a 25 MHz transducer. Each part in the figure represents a backscatter measurement from an individual different cell.

cells. This is possibly due to the presence of foreign objects in the suspension, as no concurrent microscopy of the scattering objects was available, which may have led to the erroneous interpretation of the measured backscattered pulses. These findings presented in this work lead to the conclusion that individual OCI-AML-5 cells may be modeled as fluid sphere, similarly to PC-3 prostate carcinoma cells (Baddour and Kolios, 2007) and sea urchin oocytes (Falou *et al.*, 2008) when these cells are suspended in solution. To further investigate this, each measured backscatter frequency response was compared to the theoretical response for a fluid sphere using the Anderson model. With the exception of Figs. 7(b), 7(f), and 7(g), the measured and theoretical backscatter responses follow the same trend and are of the same order of magnitude as shown in Figs. 6(a)–6(h) and 7(a)–7(h). Fluid spheres with densities ranging from 1.05 to 1.11 g/ml provided the best fit to experiment data. This is further confirmed by the fact that OCI-AML-5 cells tend to slowly settle at the bottom of the suspending medium (PBS), which implies that they have a greater density than that of PBS (1.0 g/ml).

The discrepancies in the frequency dependent backscatter, but not overall level of backscatter, found between the measured and theoretical responses in Figs. 7(b), 7(f), and 7(g) may be due to a slight deformation in the shape of the cell (difficult to observe optically) during the application of the pressure gradient along its membrane (holding process), which may have led to changes in their scattering behavior, particularly at 55 MHz, where the wavelength of the central frequency of the incident pulse approaches the size of the

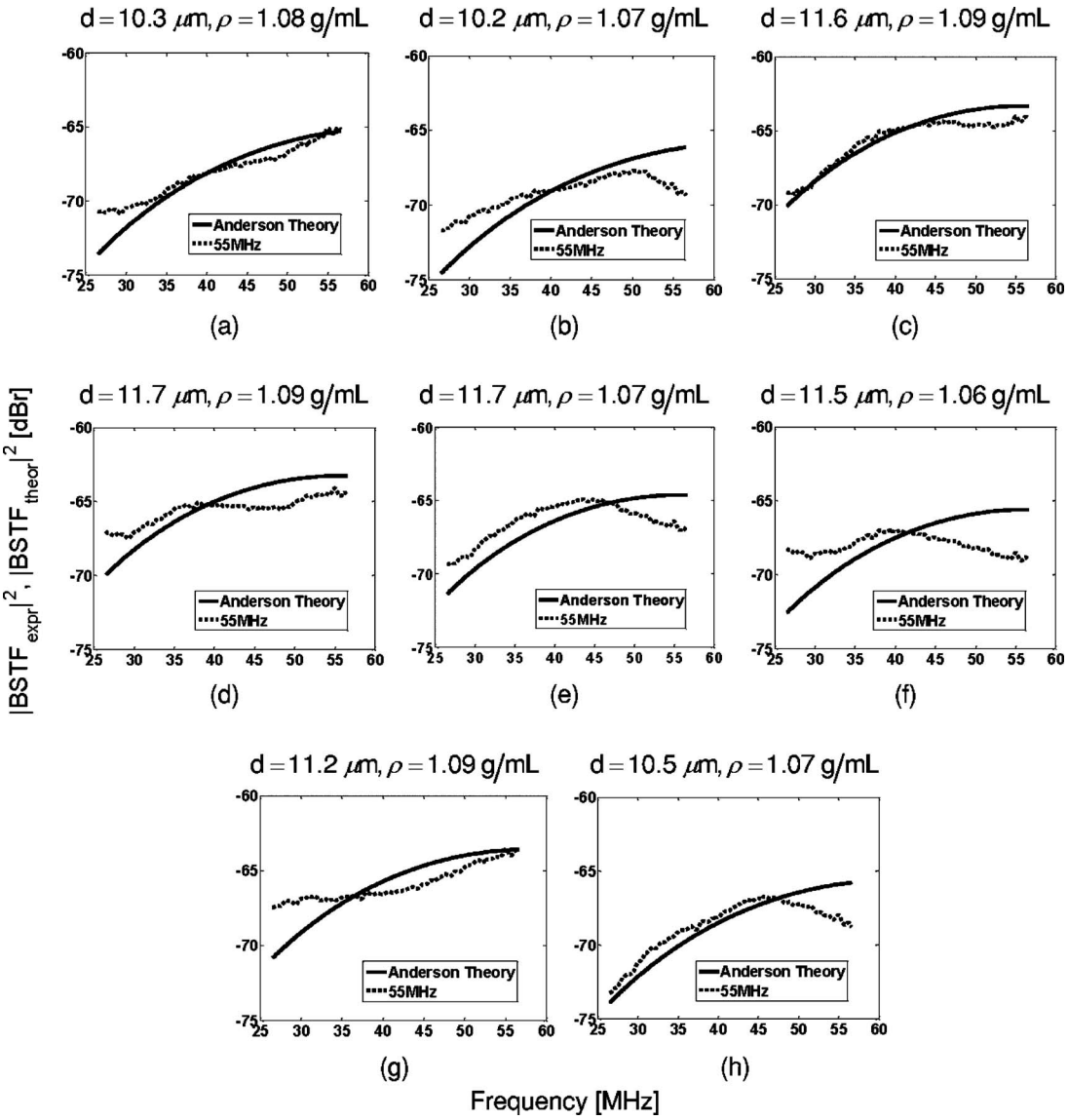

FIG. 7. Theoretical (fluid sphere model: $c=1535$ m/s, diameter and density are given in the figure title) and experimental backscatter frequency responses of a single OCI-AML-5 cell in PBS subject to incident pulses from a 55 MHz transducer. Each part in the figure represents a backscatter measurement from an individual different cell.

OCI-AML-5 cell. In addition, while every effort was made to avoid any damage to the cell by carefully employing fire-polished micropipettes, the delicate nature of the OCI-AML-5 cell membrane might have damaged the cell.

The theoretical and average experimental backscatter frequency responses presented in Fig. 8 provide a summary of the data presented in Figs. 6 and 7 and further evidence that scattering from OCI-AML-5 cells is best modeled with a fluid sphere scattering model. The theoretical backscatter predicted by the Anderson theory well agrees with experimental data within experimental error. However, it should be pointed out that cells in tissues, rather than surrounded by PBS solution, would exhibit potentially different scattering characteristics since in this configuration, it is likely that the nucleus would contribute the most to the overall scattering: the main difference in acoustical properties will be between the cytoplasm and nucleus, rather than the cell and the solution, as in these experiments (with the cytoplasm becoming the acoustic background that the PBS is in the suspension experiments). In this case, the fluid sphere model may not be an appropriate model and the scattering from the cell and nucleus may be better modeled with either more complex formulations, or models in which the elasticity of the nucleus is taken into account (Doyle *et al.*, 2009). Computer simulations may be used to calculate the ultrasound backscatter from tissues by using ultrasound scattering from collections of cells, in which each individual particles are assumed to have the same physical properties of that of the cell nucleus or that of the cell (Vlad *et al.*, 2010). This will allow for the better understanding of scattering from collections of cells such as in tumor tissues. It should be pointed out that, if the nuclei exhibited an elastic component to the scattering in tissues, other spectral features (such as peaks) that are related to the elastic nature of the nucleus (Baddour and Kolios, 2007; Doyle *et al.*, 2009), would appear in the backscattered power spectrum. However, in these suspension experiments, such spectral features have not been observed.

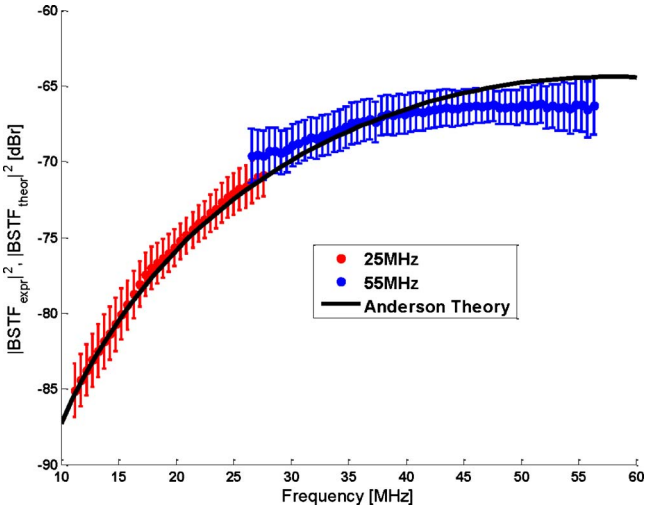

FIG. 8. (Color online) Theoretical (fluid sphere model parameters: $d=10.5$ μm, $\rho=1.09$ g/ml, $c=1535$ m/s) and average experimental backscatter frequency responses of a single OCI-AML-5 cell in PBS subject to incident pulses from two transducers: 25 and 55 MHz. Error bars represent the 95% confidence intervals. The experimental data shown correspond to the average of all data presented in Figs. 6 and 7.

The novel technique introduced in this work provided a means for measuring the exact ultrasonic backscatter response from individual micron-sized objects under optical guidance to observe the scattering object. The robustness of this technique also lies in its ability to measure the backscatter from individual cells at specific stages of apoptosis. This is particularity important for the development of theoretical models of ultrasound scattering from cell ensembles undergoing apoptosis and for the determination of the apoptotic index. Such work will help in the development of noninvasive and rapid assessment of the effectiveness of cancer therapies (Vlad *et al.*, 2008; Vlad *et al.*, 2009). This technique may also be employed in various biomedical ultrasound applications ranging from tissue characterization to molecular imaging. For instance, it can be used to study the difference between the backscatter response from individual ultrasound contrast agents in a suspending medium and individual contrast agents when they are attached to a cell.

Not all captured movies were considered appropriate for the analysis due to the following reasons: first, during the attachment of the scatterer to the micropipette, some of the suspending medium diffused into the micropipette as a result of the negative pressure applied and resulted in the failure of the release of the scatterer due to the clogging of the micropipette. Second, for delicate scatterers such as cells, a portion of the scatterer was aspired into the micropipette and resulted in damage to the cellular structure. Third, in some trials, the speed at which the scatterer left the micropipette was too high: this resulted in ultrasound frames not containing any scattering events from the object of interest. Last, since the direction which the scatterer follows upon its release from the micropipette is not controlled, the ultrasonic echoes such as the one shown in Fig. 2(f) might be captured when the scatterer and the micropipette at a very close distance, which makes it very difficult to extract the scatterer pulse from its corresponding RF line due to the overlapping of both scatterer and micropipette signals. The experimental conditions may be improved by optimizing the micropipette design (e.g., taper length, tip diameter) and the applied pressure gradient in order to prevent the aspiration of the soft scatterers into the micropipette, decrease the speed at which the scatterer gets released, and prevent physical damage to the cell.

IV. CONCLUDING REMARKS

In conclusion, the developed technique was shown to be successful in measuring the ultrasonic backscatter responses from individual micron-size objects (polystyrene microspheres) at high frequencies. The application of this technique for measuring the backscatter responses from single OCI-AML-5 cells suspended in PBS revealed that their backscatter responses at high frequencies are best modeled using the Anderson fluid sphere model. Future work will include the application of this methodology to investigate the ultrasonic behavior of a single cell at various stages of apoptosis, the behavior of contrast agents attached to cells, and the development of theoretical models to understand this behavior.

ACKNOWLEDGMENTS

The authors would like to thank Arthur Worthington and Candice Schreiber for their technical assistance, and Jonathan Mamou for suggestions on the reference phantom. This project was funded by the Canadian Institute of Health Research (Grant Nos. MOP-97959 and 79447) and Canada Research Chairs Program awarded to Michael C. Kolios and Ryerson University. The instruments used in the work were purchased with funds from the Canada Foundation for Innovation (CFI), the Ontario Ministry of Research and Innovation, and Ryerson University. O.F. is the recipient of an Ontario Graduate Scholarship (OGS) and a Graduate Research Excellence Award awarded by Ryerson University.

Anderson, V. C. (**1950**). "Sound scattering from a fluid sphere," J. Acoust. Soc. Am. **22**, 426–431.

Baddour, R. E., and Kolios, M. C. (**2007**). "The fluid and elastic nature of nucleated cells: Implications from the cellular backscatter response," J. Acoust. Soc. Am. **121**, EL16–EL22.

Baddour, R. E., Sherar, M. D., Hunt, J. W., Czarnota, G. J., and Kolios, M. C. (**2005**). "High-frequency ultrasound scattering from microspheres and single cells," J. Acoust. Soc. Am. **117**, 934–943.

Czarnota, G. J., Kolios, M. C., Abraham, J., Portnoy, M., Ottensmeyer, F. P., Hunt, J. W., and Sherar, M. D. (**1999**). "Ultrasound imaging of apoptosis: High-resolution non-invasive monitoring of programmed cell death in vitro, in situ and in vivo," Br. J. Cancer **81**, 520–527.

Czarnota, G. J., Kolios, M. C., Vaziri, H., Benchimol, S., Ottensmeyer, F. P., Sherar, M. D., and Hunt, J. W. (**1997**). "Ultrasonic biomicroscopy of viable, dead and apoptotic cells," Ultrasound Med. Biol. **23**, 961–965.

Doyle, T. E., Tew, A. T., Warnick, K. H., and Carruth, B. L. (**2009**). "Simulation of elastic wave scattering in cells and tissues at the microscopic level," J. Acoust. Soc. Am. **125**, 1751–1767.

Falou, O., Baddour, R. E., Nathanael, G., Czarnota, G. J., Kumaradas, J. C., and Kolios, M. C. (**2008**). "A study of high frequency ultrasound scattering from non-nucleated biological specimens," J. Acoust. Soc. Am. **124**, EL278–EL283.

Faran, J. J. (**1951**). "Sound scattering by solid cylinders and spheres," J. Acoust. Soc. Am. **23**, 405–418.

Feleppa, E. J., Liu, T., Lizzi, F. L., Kalisz, A., Silverman, R. H., Sigel, B., and Fair, W. R. (**2000**). "Three-dimensional ultrasonic parametric and tissue-property imaging for tissue evaluation, treatment planning, therapy

guidance, and efficacy assessment," in Proceedings of SPIE—The International Society for Optical Engineering, San Diego, CA, pp. 68–76.
Häcker, G. (**2000**). "The morphology of apoptosis," Cell Tissue Res. **301**, 5–17.
Hunt, J. W., Worthington, A. E., Xuan, A., Kolios, M. C., Czarnota, G. J., and Sherar, M. D. (**2002**). "A model based upon pseudo regular spacing of cells combined with the randomisation of the nuclei can explain the significant changes in high-frequency ultrasound signals during apoptosis," Ultrasound Med. Biol. **28**, 217–226.
Insana, M. F., and Hall, T. J. (**1990**). "Characterizing the microstructure of random-media using ultrasound," Phys. Med. Biol. **35**, 1373–1386.
Kerr, J. F. R., Wyllie, A. H., and Currie, A. R. (**1972**). "Apoptosis—Basic biological phenomenon with wide-ranging implications in tissue kinetics," Br. J. Cancer **26**, 239–257.
Kolios, M. C., Czarnota, G. J., Worthington, A., Giles, A., Tunis, A. S., and Sherar, M. D. (**2004**). "Towards understanding the nature of high frequency backscatter from cells and tissues: An investigation of backscatter power spectra from different concentrations of cells of different sizes," in Proceedings of the 2004 IEEE International Ultrasonics, Ferroelectrics, and Frequency Control Joint 50th Anniversary Conference, Montreal, Quebec, Canada, pp. 606–609.
Lizzi, F. L., Astor, M., Feleppa, E. J., Shao, M., and Kalisz, A. (**1997**). "Statistical framework for ultrasonic spectral parameter imaging," Ultrasound Med. Biol. **23**, 1371–1382.
Lizzi, F. L., Greenebaum, M., Feleppa, E. J., Elbaum, M., and Coleman, D. J. (**1983**). "Theoretical framework for spectrum analysis in ultrasonic tissue characterization," J. Acoust. Soc. Am. **73**, 1366–1373.
Lizzi, F. L., King, D. L., Rorke, M. C., Hui, J., Ostromogilsky, M., Yaremko, M. M., Feleppa, E. J., and Wai, P. (**1988**). "Comparison of theoretical scattering results and ultrasonic data from clinical liver examinations," Ultrasound Med. Biol. **14**, 377–385.
Mamou, J., Oelze, M. L., O'Brien, W. D., and Zachary, J. F. (**2006**). "Perspective on biomedical quantitative ultrasound imaging," IEEE Signal Process. Mag. **23**, 112–116.
Oelze, M. L., Zachary, J. F., and O'Brien, W. D., Jr. (**2002**). "Characterization of tissue microstructure using ultrasonic backscatter: Theory and technique for optimization using a Gaussian form factor," J. Acoust. Soc. Am. **112**, 1202–1211.
Saraste, A., and Pulkki, K. (**2000**). "Morphologic and biochemical hallmarks of apoptosis," Cardiovasc. Res. **45**, 528–537.
Taggart, L. R., Baddour, R. E., Giles, A., Czarnota, G. J., and Kolios, M. C. (**2007**). "Ultrasonic characterization of whole cells and isolated nuclei," Ultrasound Med. Biol. **33**, 389–401.
Tunis, A. S., Czarnota, G. J., Giles, A., Sherar, M. D., Hunt, J. W., and Kolios, M. C. (**2005**). "Monitoring structural changes in cells with high-frequency ultrasound signal statistics," Ultrasound Med. Biol. **31**, 1041–1049.
Ursea, R., Coleman, D. J., Silverman, R. H., Lizzi, F. L., Daly, S. M., and Harrison, W. (**1998**). "Correlation of high frequency ultrasound backscatter with tumor microstructure in iris melanoma," Ophthalmology **105**, 906–912.
Vlad, R. M., Alajez, N. M., Giles, A., Kolios, M. C., and Czarnota, G. J. (**2008**). "Quantitative ultrasound characterization of cancer radiotherapy effects in vitro," Int. J. Radiat. Oncol., Biol., Phys. **72**, 1236–1243.
Vlad, R. M., Brand, S., Giles, A., Kolios, M. C., and Czarnota, G. J. (**2009**). "Quantitative ultrasound characterization of responses to radiotherapy in cancer mouse models," Clin. Cancer Res. **15**, 2067–2075.
Vlad, R. M., Saha, R. K., Alajez, N. M., Ranieri, S., Czarnota, G. J., and Kolios, M. C. (**2010**). "An increase in cellular size variance contributes to the increase in ultrasound backscatter during cell death," Ultrasound Med. Biol. (in press).